Effect of Fracture Mode on Acoustic Emission Behavior in the Hydrogen Embrittled Low-Alloy Steel

E.D. Merson[1], P.N. Myagkikh[1], G.V. Klevtsov[1], D.L. Merson[1], A. Vinogradov[2]

[1]*Institute of Advanced Technologies, Togliatti State University, Belorusskaya str. 14, Togliatti 445667, Russian Federation*

[2]*Department of Mechanical and Industrial Engineering, Norwegian University of Science and Technology – NTNU, N-7491 Trondheim, Norway*

Abstract

Hydrogen embrittlement (HE) of steels and other alloys is a long-standing scientific and engineering problem causing sudden premature failures of industrial components. Although several mechanisms of hydrogen-assisted cracking (HAC) have been proposed, there is still neither commonly accepted agreement on the exact role of hydrogen in this process nor the reliable way to recognize the operating mechanism of HAC. In the present paper, we endeavor to demonstrate that the acoustic emission (AE) technique is a promising tool for in-situ investigating of HAC mechanisms and distinguishing between them. The experiments were performed using the low-alloy steel grade 09G2S obtained in the low-strength as-received state and the high-strength state after severe plastic deformation by equal channel angular pressing (ECAP). The specimens of both kinds were tensile tested before and after hydrogen charging as well as after removing diffusible hydrogen for evaluation of the influence of hydrogen induced cracks (HICs). It is established that HICs, which are formed during hydrogen charging, do not affect the mechanical properties, fracture surface topology and the AE behavior in both as-received and ECAPed specimens, provided that diffusible hydrogen is removed from the steel. Two different kinds of HAC were observed. The first operated in the as-received low-strength steel; it produced weak AE response and was featured by the formation of fisheyes defects with quasi-cleavage morphology. The second type of HAC was observed in the ECAPed high-strength steel; it generated high-energy AE signals and was featured by the formation of mixed torn/cleavage morphology on the fracture surface. Obtained results are discussed and explained from the viewpoint of the known mechanisms of HAC including hydrogen-enhanced localized plasticity (HELP), hydrogen enhanced decohesion (HEDE) and others.

Keywords: hydrogen embrittlement, acoustic emission, equal channel angular pressing; severe plastic deformation, fractography, quasi-cleavage, hydrogen assisted cracking, low-alloy steel, fisheyes.

1.   Introduction

Failures of steel components due to hydrogen embrittlement (HE) are omnipresent and everlasting in the industry [1]. The complete elimination of such failures is difficult because of the high cost of materials that are immune to HE. In turn, the development of economic ways to increase the resistance of steels to HE is impeded by the complexity of this phenomenon which has not been comprehensively understood up to date despite significant efforts in the field. Since the driving mechanism of HE is unclear, it is impossible to construct a reliable predictive model, which makes it challenging to forecast the service life and, therefore, to plan maintenance of steel equipment operating in hydrogen-bearing environments.

It has been well established that hydrogen dissolved in a steel matrix can recombine into molecules, producing high local pressure in bulk and causing hydrogen-induced cracking (HIC). Alternatively, if hydrogen remains in a diffusible protonic form, it can activate and facilitate crack growth, which is referred to as hydrogen-assisted cracking (HAC). The latter requires external stress and is accompanied by the change in the fracture mode from ductile to brittle (at least by visual evaluation). Several theories have been proposed to explain the nature of HAC [2–4]. Despite the difference in details, the proposed mechanisms can be divided into two substantially different groups – "brittle" and "ductile". The first group of models implies that hydrogen induces brittle fracture through the reduction of interatomic bonds strength due to the hydrogen-enhanced decohesion (HEDE) mechanism [5,6] or due to suppressing of the dislocation emission from the crack tip [7]. Both mechanisms assume that brittle cracking occurs when the critical concentration of diffusible hydrogen is attained locally [6,7] (particularly at the crack tip). It is believed that at such a hydrogen concentration, the stress required for brittle fracture becomes lower than that needed for dislocation emission ensuring stress relaxation by crack tip blunting. If any of these mechanisms operate, the fracture mode should be similar to the conventional brittle fracture such as that observed for a given material due to cold embrittlement. Usually, this approach applies to explain the HE phenomenon in high-strength steels exhibiting cleavage or intergranular fracture surfaces. The second group of models has footed on the premise that hydrogen promotes and modifies the microvoid-coalescence (MVC) fracture mode due to the interaction of atomic hydrogen with other crystallographic defects. Hydrogen-enhanced localized plasticity (HELP) [2] and adsorption-induced dislocation emission (AIDE) [3] mechanisms imply that hydrogen facilitates and localizes dislocation processes in bulk or in the vicinity of the free surface, respectively. The vacancy-induced nanovoid nucleation and coalescence (NVC) theory [4] considers stabilization of vacancies by hydrogen as a key factor causing a premature fracture. According to these theories, the fracture surface of the hydrogen

embrittled metals is only seemingly brittle. On the fine scale, it consists of shallow dimples, tear ridges and other features typical of the locally plastic behavior. In particular it is believed that these mechanisms can be responsible for the formation of specific quasi-cleavage fracture surfaces referred to also as "cleavage-like" or "quasi-brittle", which are usually found in the low-strength materials such as pure iron and low-carbon steels. Martin et al. [8] concluded that the formation of quasi-cleavage morphology in hydrogen embrittled low-carbon steel is assisted by the HELP mechanism and is advanced by nucleation, growth, and coalescence of micropores at the intersection of slip planes. Based on the AIDE theory, Lynch proposed that seemingly flat cleavage-like fracture surfaces consist in fact of nano-dimples and are produced by facilitated coalescence of the crack with nano-voids. Neeraj et al. [9] indeed found the nano-dimples on quasi-brittle facets in ferritic steels. However, they suggested that this relief can arise from the NVC mechanism. Although many results [3,8–13] supporting the existence and even coexistence and synergistic interplay [14–16] of the all theories above have been reported recently, there are no reliable techniques capable for recognizing the operating mechanisms of HAC and distinguishing between them.

The modern acoustic emission (AE) method might be one of the most promising tools for this purpose. With its outstanding sensitivity to elementary processes of plastic deformation and fracture including dislocation slip and twinning [17,18], crack nucleation and growth [19,20], etc., AE provides a unique opportunity for real-time non-destructive monitoring and assessment of damage accumulation processes including HAC. It is plausible to expect that "brittle" and "ductile" HAC mechanisms mentioned above should exert substantially different effects on AE behavior. In particular, it is known that dislocation-mediated plastic deformation processes and MVC fracture are usually accompanied by continuous noise-like AE with a quite low energy/power in contrast with common brittle cleavage or intergranular fracture which is featured by burst type high-energy AE signals.

Indeed, contradictory results have been reported with regard to the effect of HE on AE, depending on the material and experimental conditions. Although convincing evidences exist for the strong high-amplitude AE signals produced by advancing cracks in steels embrittled by hydrogen [21–28], either no change or even reduction of the AE amplitude and activity have been observed in some steels after hydrogen charging while the fracture mode has altered from ductile to brittle and the ductility has dropped [29,30]. The high-amplitude burst type AE was mainly observed during intergranular HAC in high-strength martensitic steels 4340 [22,27] and 300M [24], austenitic stainless steel 304 [25,26,31], high-carbon steels grade 70 [28,32], U8 [33] and others [25], and also in iron with P segregated at grain boundaries [25,31]. Vasudevan et al. [23] have found that the intergranular fracture of the 0.05C microalloyed steel welds is a weaker

source of AE than the transgranular quasi-cleavage fracture in the welded 0.26C-Mn steel when both steels were saturated with hydrogen. In contrast You et al. [29] have shown that hydrogen charging of the low-carbon 2.25Cr–1Mo steel led to appearance of quasi-cleavage regions in the fracture surface, which accompanied by the decrease in the AE energy in the yield plateau region during tensile testing. Merson et al. [30] have observed no significant change in the AE behavior after hydrogen charging of the low-carbon steel S235JR though the drop of the tensile elongation at break and the appearance of fisheye defects with the quasi-cleavage morphology on the fracture surface were found.

The literature survey shows that there is a trend to observe a higher AE response from intergranular HAC in high-strength and high-carbon steels than that from quasi-cleavage in mild and low-carbon steels. This is exactly what one expects if HAC occurs either by "brittle" or "ductile" mechanisms in high- or low-strength steels, respectively. However, at present, it is not possible to establish any quantitative relationship or even a correlation between AE parameters and features of HAC because the all aforementioned studies were performed at different experimental conditions including chemical compositions of materials, the hydrogen charging and mechanical testing methods, specimen geometry and size, settings and types of AE equipment, etc. In order to establish the relationship between the HAC fracture mode and the AE behavior, these factors should be kept the same in a series of experiments. To the author's best knowledge, no direct comparison of AE features arising from different fracture modes in the hydrogen embrittled steel at the same experimental conditions has been performed up to date. Thus, the main objective of the present study is to assess the effect of fracture mode on the AE behavior in the hydrogen embrittled low-alloy steel.

2.   Experimental

The commercial low-carbon low-alloy steel grade 09G2S manufactured in accordance with the GOST 27772-88 standard was received as hot-rolled bars of 20 mm diameter. The chemical composition of this steel is close to EU analogs - 13Mn6 (Germany) or VH2 (Hungary) and is provided in Table 1. When hydrogen charged in the as-received state this steel is prone to quasi-cleavage fracture similarly to other low-strength steels. To promoted an alternative fracture mode, the as-received steel was significantly strengthened through the thermo-mechanical treatment including the following steps: 1) homogenizing annealing at 810 °C followed by quenching in water, 2) tempering at 450 °C, 3) cold severe plastic deformation by "CONFORM" equal-channel angular pressing (ECAP) to 4 passes by the Bc route and 4) annealing at 350 °C for residual stress removing[1]. During the past 3 decades ECAP has become a popular pathway for manufacturing bulk ultra-fine grained materials with a combination of remarkably high

---

[1] All treatments concerning to ECAP were conducted in the Ufa State Aviation Technical University

strength and reasonable ductility (though the latter is often below expectations). The comprehensive review on the principles, advantages and disadvantages of this technique can be found elsewhere [34]. In the present study, the ECAP-based treatment was employed to obtain the high-strength steel with the same chemical composition as in the low-strength as received state. The as-received (hot-rolled) and ECAPed bars were longitudinally sliced to 2.4 mm thick plates by the electrical discharge machine. They were then grounded down to 2.1 mm thick. Flat and smooth specimens for tensile testing with 4x15 mm^2 gage dimensions were cut from the obtained plates and grounded by emery paper #240.

Table 1 – Chemical composition of the steel grade 09G2S (GOST 27772-88).

Elements, w. %										
C	Si	Mn	P	S	Cr	Ni	Cu	V	Al	Fe
0.091	0.722	1.358	0.016	0.011	0.097	0.072	0.235	<0.005	0.018	Base

Cathodic hydrogen charging was performed in 5% H_2SO_4 + 1.5 g/l of thiourea solution at 20 mA/cm^2 current density during 1 hour. Platinum wire was used as an anode. Within 5 minutes after hydrogen charging the specimens were washed in running water, dried by hot air, rinsed in CCl_4 and subjected to tensile testing.

Hydrogen charging can produce the hydrogen-induced cracks (HICs) even without any external stress. Serving as stress risers, the HICs might affect the fracture mode without assistance of diffusible hydrogen, especially in the high-strength steel. In order to evaluate the influence of irreversible damage produced by hydrogen charging, the diffusible hydrogen was removed from several as-received and ECAPed specimens before tensile testing. To remove diffusible hydrogen and to measure its concentration, the annealing was performed by the inert carrier gas hot-extraction method in the gas-analyzer Galileo G8 (Bruker). The specimen was heated in a quartz tube with the flowing pure nitrogen carrier gas. Hydrogen extracting from the specimen was carried out by the flux of pure nitrogen to the thermal conductivity detector where hydrogen concentration was determined by the difference between thermal conductivities of pure nitrogen and its mixture with extracted hydrogen. Each specimen was heated up to 200 °C with the heating rate of 17 °C/min and held at the destination temperature for 15 min. One of the hydrogen-charged ECAPed specimens was also degassed in a two step procedure comprising of holding at 200 °C for 30 minutes followed by 5 min holding at 300 °C. These two regimes of degassing will be further referred to as "degassing at 200 °C" and "degassing at 300 °C". It was not possible to confirm that diffusible hydrogen was completely removed from the steel by these procedures. However, one can say with confidence that at least its concentration should be

substantially reduced. The concentration of diffusible hydrogen in the specimens, which were not degassed before tensile testing, was determined after tensile test by degassing at 200 °C in the gas analyzer.

Thus, three batches of specimens were used for tensile testing: (i) "not charged" – the specimens which were not subjected to hydrogen charging, (ii) "hydrogen charged" and (iii) "degassed" – the hydrogen-charged specimens which were degassed before tensile testing. All specimens were tensile tested using a screw-driven testing frame with the crosshead velocity of 5 mm/min ($6 \cdot 10^{-3}$ s^{-1}).

To promote the conventional purely brittle fracture mode, the standard Charpy tests on the not charged as-received and ECAPed specimens having a V-shape notch and 10x10x55 mm^3 dimensions were conducted in accordance with the ASTM A370 standard at liquid nitrogen temperature for comparison.

Raw AE data were recorded during the tensile tests in the continuous threshold-less mode using a broadband (200-750 kHz) piezoelectric sensor Pico (Physical Acoustics Corporation, PAC) mounted on the specimen through the grease. The signal from the transducer was amplified by 60 dB using the low-noise 2/4/6 (PAC) 30-1300 kHz amplifier and then fed to 16 bits ADC PCI-2 (PAC) operated with the sampling rate set as 2 MHz and additional amplification set as 6 dB. Using the home-made software, the acquired streams were sectioned into successive realizations ("frames") of 2 ms duration. A power spectral density (PSD) function was calculated for each frame using a conventional Welch technique. The average energy, E_{AE}, per frame were calculated in the frequency domain. For every test, the total AE energy accumulated during the whole test, ΣE_{AE}, and before fracture, ΣE^F_{AE}, was calculated as a sum of energies of all AE frames with energy exceeding that of AE frames corresponding to the background noise. The curves of E_{AE} accumulation during the test were plotted as a function of strain or time.

Examination of the microstructure and morphology of side surfaces and fracture surfaces was performed using a filed-emission gun scanning electron microscope (SEM) SIGMA (Carl Zeiss) equipped with the EDAX/TSL Hikari XP electron back scattering diffraction (EBSD) detector. The standard RD (rolling or extrusion direction), TD (transverse direction) and ND (normal direction) designations of planes were used for the metallographic study.

3.   Results

3.1. Effect of hydrogen charging on microstructure and surface before tensile testing

As-received specimens have a typical ferrite-perlite microstructure with coarse equiaxial ferritic grains of 10 μm average diameter, as can be seen in Fig. 1a. The wide assortment of non-metallic inclusions such as Al_2O_3 or elongated sulfides MnS is abundantly present in the microstructure, c.f. Fig. 2a, b.

After hydrogen charging, the surface of the as-received specimens contains blisters, Fig. 2c, which are the regions of the inflated metal surface with underlying HICs, see white arrows in Fig. 2d. The HICs are oriented primarily along the rolling direction of steel. They probably originate at non-metallic inclusions/matrix interfaces or grain boundaries but ones nucleated they grow transgranularly across the ferritic grains, as clearly shown in Fig. 2d.
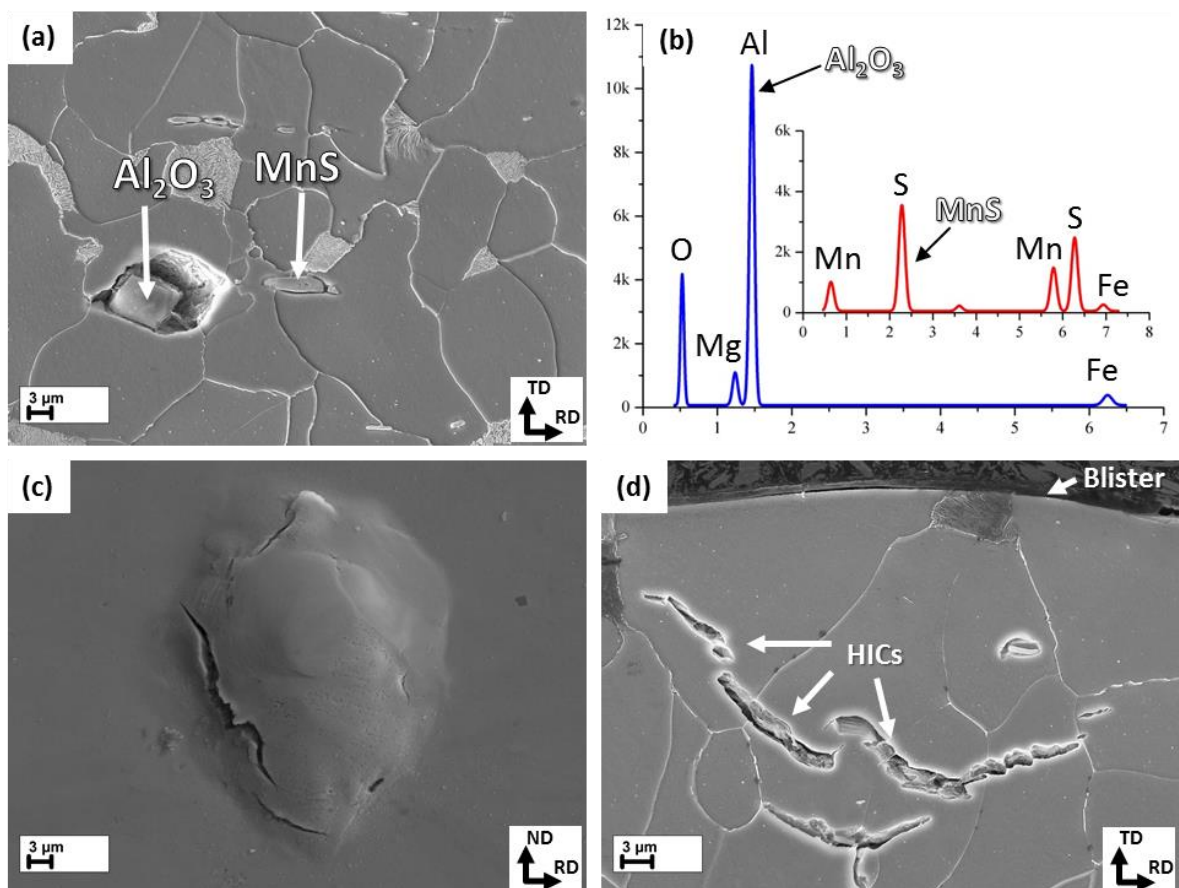

Fig. 1 – Microstructure – (a), Energy Dispersion X-ray (EDX) spectra – (b) for the non-metallic inclusions seen in (a), hydrogen-induced blisters on the surface – (c) and hydrogen-induced cracks in the microstructure – (d) of the as-received steel.

When examined by conventional SEM, the etched polished surface of the ECAPed steel demonstrates a distorted ferrite-pearlite microstructure with slightly smaller ferritic grain size in comparison with that in as-received steel, Fig. 2a. Grains are elongated in the direction of ~45° to the extrusion direction, which is a common feature of many ECAPed microstructures. Nevertheless, the orientation map obtained by the EBSD technique and inked in inverse pole figure (IPF) colors shows that during ECAP the steel undergoes severe plastic deformation resulting in substantial grain refinement, Fig. 2b. The microstructure exhibiting a pronounced macroscopic texture is composed of small grains or sub-grains with the average diameter of 0.6 μm. Dislocation-based low-angle grain boundaries are clearly seen in the original grains where transformation of the microstructure into the ultra-fine grained one has not been completed.

The thin near-surface HICs (but no blisters) have been observed in the hydrogen-charged ECAPed specimens, Fig. 2c, d. All of them are primarily transgranular and are oriented at approximately 45° to the extrusion direction of the steel. Thus, they are aligned with the primary direction of grains elongation which occurs in the shear plane of the last pressing operation.
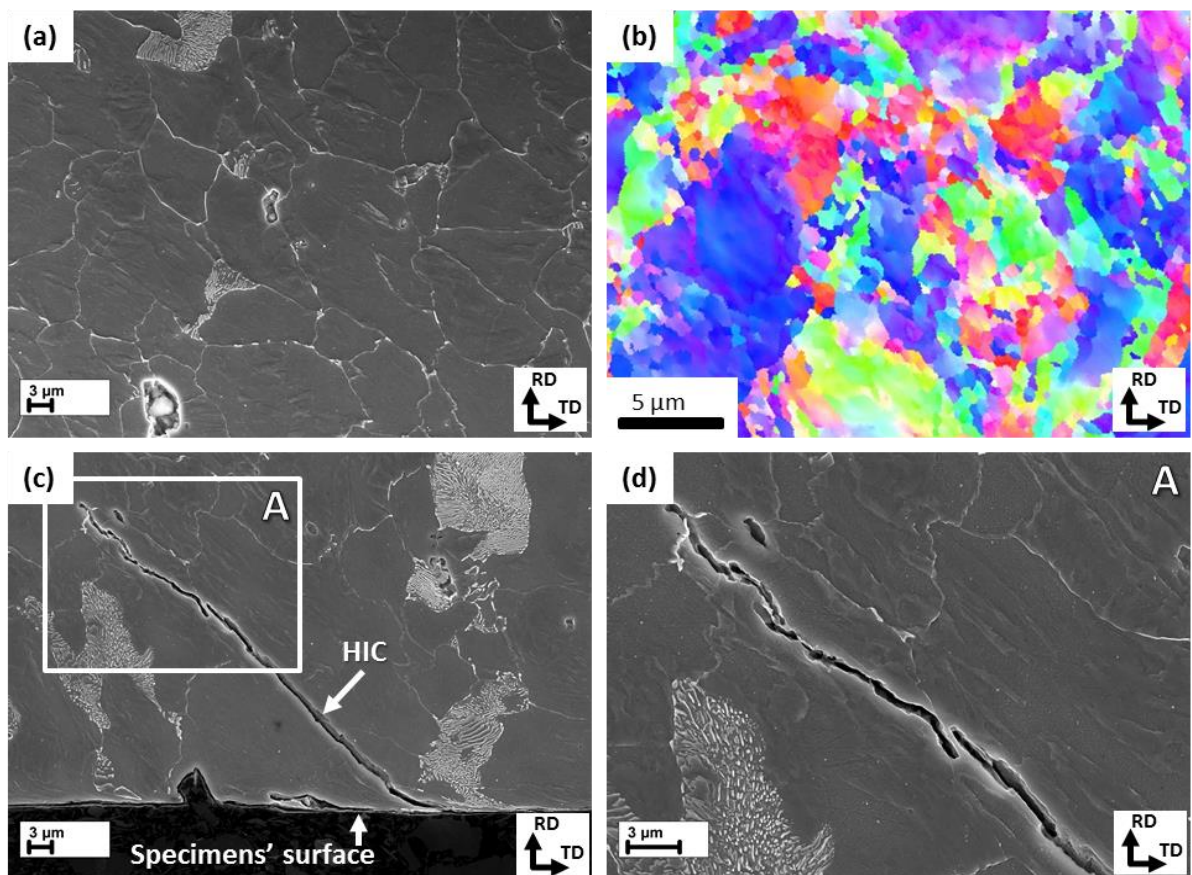

Fig. 3 – Microstructure – (a, b) and hydrogen-induced cracks (e, f) of the ECAPed steel grade 09G2S. (a, c, d) – SEM, (b) – Inverse Pole Figure (IPF) colored orientation map obtained by the EBSD method. A magnified view of the region labeled by A is shown in (d).

3.2. Effect of hydrogen charging on hydrogen concentration

According to the results of the gas-analysis presented in Table 2, the concentrations of diffusible hydrogen before (C^I_H) and after (C^R_H) tensile testing are similar. All specimens contain the quite high diffusible hydrogen concentration. It is however much higher in the ECAPed specimens (of 11 ppm) than in the as-received ones (of 2 ppm).

3.3. Effect of hydrogen charging on mechanical properties

The stress-strain diagrams of the not charged as-received specimens demonstrate the region of quasi-elastic deformation followed by a pronounced yield plateau with a stress drop in the beginning and the strain hardening commencing at the end of the plateau, Fig. 3a.

As follows from Table 2 the hydrogen charging of the as-received specimens results in the decrease of their elongation, which is compromised mainly due to shortening of the necking stage, Fig. 3c. Nevertheless, the fracture of the as-received specimens is always preceded by appreciable localized deformation in the neck. Removing of diffusible hydrogen from the as-received steel before tensile testing results in the complete recovery of mechanical properties and the shape of the stress-strain diagram, c.f. Table 2 and Fig. 3e.

Table 2 – Initial C^I_H and residual C^R_H concentration of diffusible hydrogen, tensile properties and AE characteristics of the steel grade 09G2S in the as-received and ECAP states before and after hydrogen charging.[2]

Specimen type	As-received			ECAP			
	Not charged	Hydrogen charged	Degassed at 200 °C	Not charged	Hydrogen charged	Degassed at 200 °C	Degassed at 300 °C
C^I_H, ppm	-	-	2.0	-	-	10.7	11.0
$C^R_{H,}$ ppm	-	2.0± 0.2	-	-	11.7 ± 2.8	-	-
δ, %	39.8 ± 1.2	27.9 ± 0.1	39.6	13.1 ± 0.2	0.7 ± 0.2	10.9	13.3
$\sigma_{UTS,}$ MPa	485 ± 3	492 ± 2	489	837 ± 12	701 ± 4	827	831
ΣE_{AE}, arb. units	4.5 ± 1.8	5.1 ± 1.7	4.8	18.8 ± 11.6	106.8 ± 25.2	6.5	13.8
ΣE^F_{AE}, arb. units	4.1± 1.6	4.1± 0.7	4.5	0.0022± 0.0002	90.3± 28.6	0.4	0.14

[2] The standard deviations presented in the table after "±" sign were determined using results for 2-4 specimens tested at the same conditions. If standard deviations are not shown, the results were obtained from one specimen.

The ECAP results in the substantial increase of the steel strength but the elongation is compromised, Table 2. The stress-strain behavior is also changed, so that the yield plateau vanishes completely, and both the strain hardening stage and the necking stage shorten, Fig. 3b.

After hydrogen charging the fracture of the ECAPed specimens occurs suddenly in the region of quasi-elastic deformation or at the very beginning of the strain-hardening stage, so that the strain at fracture does not exceed 1 %, Fig. 3d. Degassing at 200 °C for 30 minutes followed by 5 minutes additional annealing at 300 °C completely recovers the mechanical properties of the hydrogen-charged ECAPed steel, c.f. Table 2. The shorter degassing at a lower temperature is less effective. It also remarkably reduces the harmful effect of hydrogen charging on ECAPed steel properties, Fig. 3f.
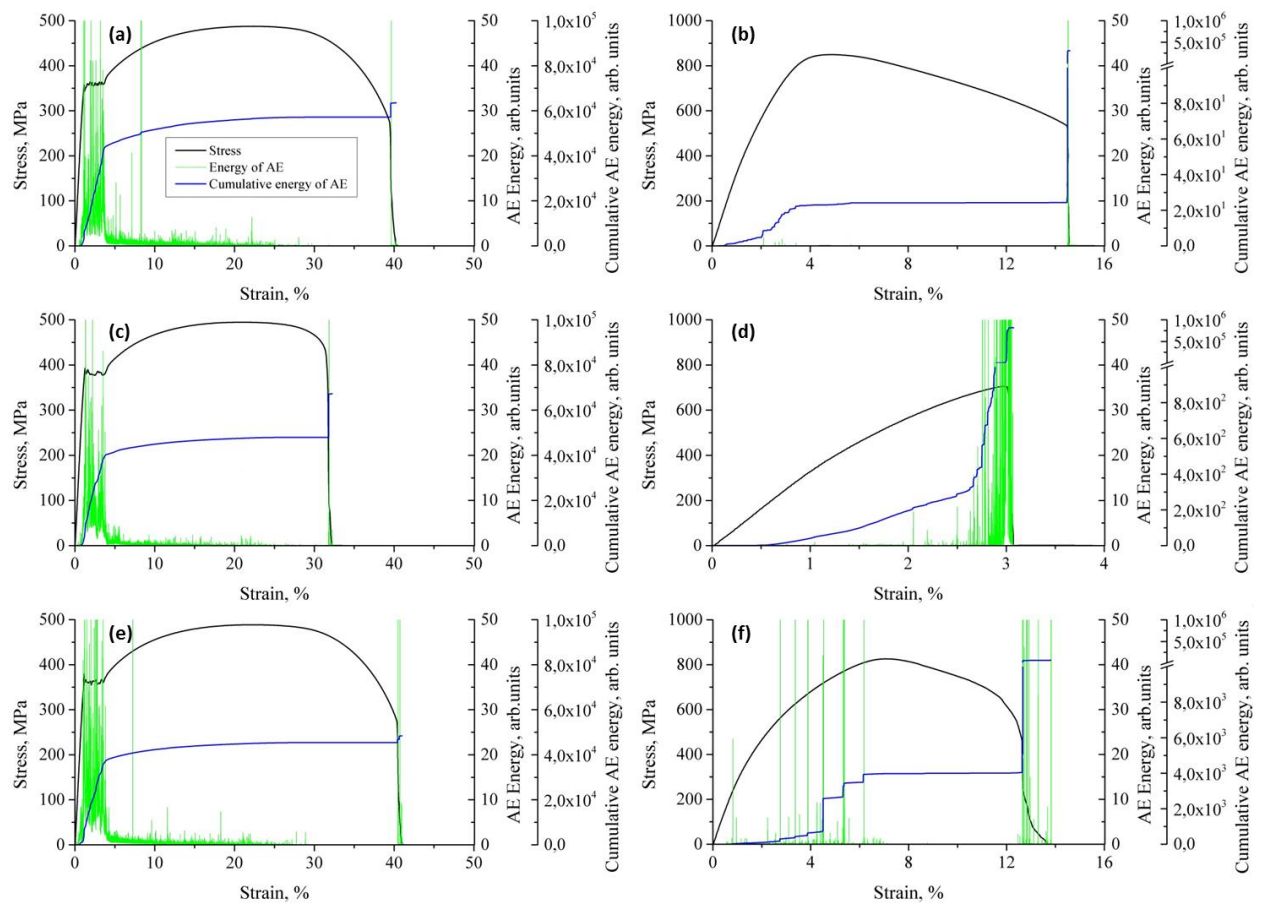

Fig. 3 – Stress-strain diagrams and concomitant AE behavior - AE energy values and AE energy accumulation curves - for the as-received - (a, c, e) and ECAPed - (b, d, f) specimens tensile tested before - (a, b) and after hydrogen charging (c, d) and after hydrogen charging and degassing at 200 °C for 15 minutes - (e, f).

3.4. Effect of hydrogen charging on acoustic emission

The AE behavior during tensile tests of the not charged as-received specimens is typical for low-carbon steels, see Fig. 3a. The highest rate of AE energy accumulation is observed during the yielding stage. After sharp peaking, the AE activity reduces during the strain hardening stage until fracture that is accompanied by strong AE transients as illustrated in Fig. 3a. Throughout the test AE appears as a mixture of continuous noise-like and discrete burst type signals. It has been well established that continuous AE in such steels is produced by cooperative dislocation movement while the burst-type AE is often associated with fracture of non-metallic inclusions or cementite lamellas [35].

It is interesting that hydrogen charging of the as-received specimens does not result in any notable change in the AE behavior, see Fig. 3c, despite the fact that HE has occurred and manifested itself through mechanical properties, and many alternations in the microstructure and fracture surface (see discussions above and below in the text). As follows from Table 2, before and after hydrogen charging the total AE energies accumulated during plastic deformation before fracture, ΣE^F_{AE}, and during the whole test of the as-received specimens, ΣE_{AE}, are approximately the same within the regular scatter. The degassing procedure also does not result in any notable change in the AE behavior, as can be seen in Fig. 3e and Table 2.

Negligible AE has been detected during tensile testing of the fine grained ECAPed specimens before hydrogen charging except the final fracture stage when strong AE impulses emerge, see Fig. 3b and Table 2. Obviously the lack of AE is explained by severe cold working of the steel caused by ECAP so that plastic deformation processes are limited and do not produce measurable AE in a severely hardened ECAPed material [36] in good agreement with the Kaiser effect.

The hydrogen charging of ECAPed specimens results in the appearance of high-energy transient AE signals, Fig. 3d. The AE activity in this case starts shortly after the onset of loading during the quasi-elastic deformation. It then dramatically increases shortly before final fracture which is accompanied by the large AE energy release. The total AE energy accumulated before the onset of fracture is found by four orders of magnitude higher than that before hydrogen charging and about 20 times higher than that in the as-received specimens, Table 2.

The degassing process leads to decrease of the AE intensity which becomes most pronounced just before necking and during fracture, see Fig. 3f. The ΣE_{AE} and ΣE^F_{AE} values are substantially lower than in the initial non-degassed specimens, Table 2. Nevertheless the intensity of AE in the degassed ECAPed specimens is still much higher than in the not charged ones. Besides, it depends on the effectiveness of degassing. As follows from Table 2, the degassing at higher temperature and longer time results in better recovery of mechanical properties concomitant with the lower total AE energy accumulated before fracture.

3.5.Effect of hydrogen charging on the fracture surface and the underlying microstructure

All tensile tested specimens, which were not charged with hydrogen, exhibit entirely ductile fracture with the dimpled fracture surface, c.f. Fig. 4. Dimples are preferably nucleated around nonmetallic inclusions, as can be seen in Fig. 4c, d.
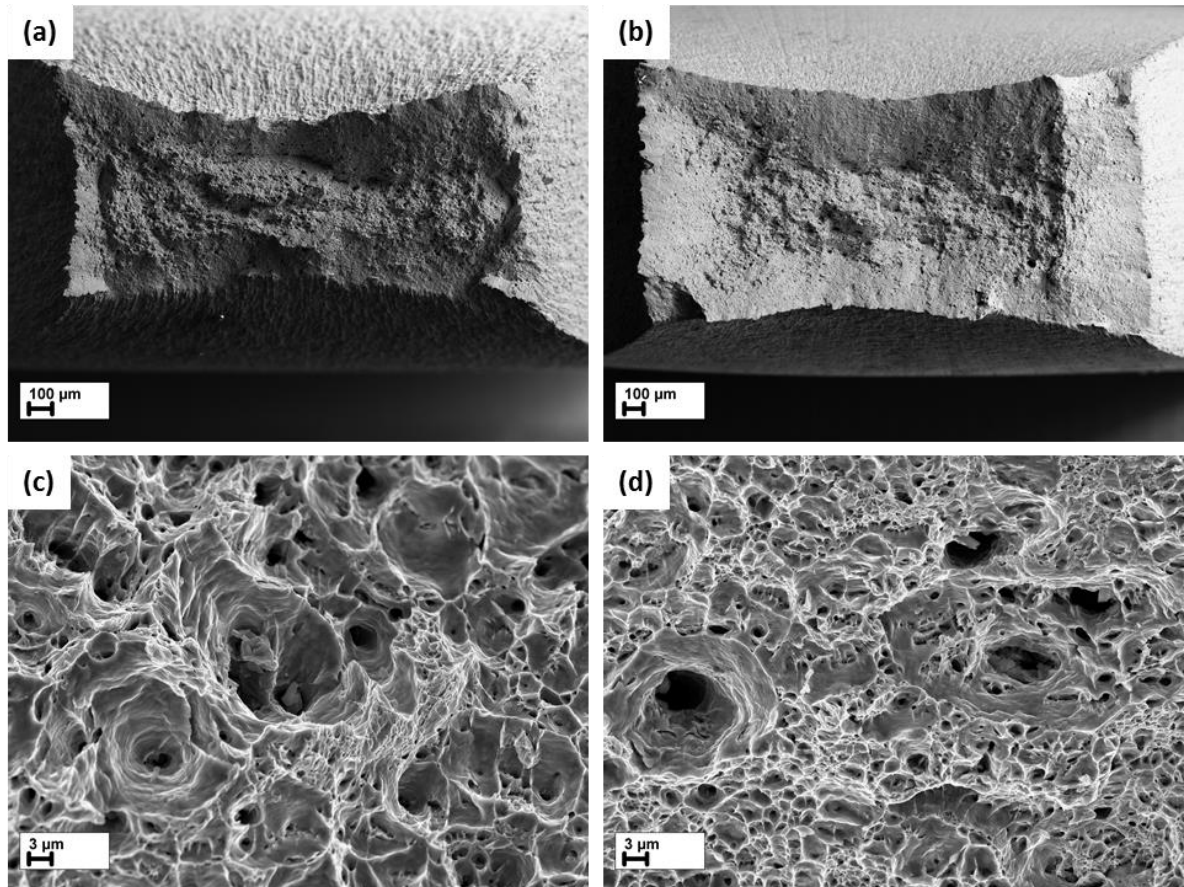

Fig. 4 – Fracture surfaces of the as-received (a, c) and ECAPed (b, d) specimens tensile tested before hydrogen charging: full-scale views (a, b) and magnified fragments (c, d).

Both type specimens impact tested in liquid nitrogen demonstrate brittle fracture surfaces, c.f. Fig. 5. The fracture surface of the as-received specimens exhibits the regular transgranular cleavage facets with typical river patterns and pronounced boundaries, Fig. 5a. In the case of ECAPed steel, the fracture surface is composed of brittle terraces, Fig. 5b, which are linked by the walls having a ductile dimpled relief, Fig. 5c. The morphology of the brittle terraces primarily consists of cleavage facets. These facets appear highly distorted. However, they still exhibit clear cleavage features such as river lines originating at the facets boundaries, Fig. 5d, e. The minor part of the brittle relief is presented by smoothly curved regions with tear ridges, Fig. 5d, f. The larger areas having a similar morphology have been found close to the periphery of the

fracture surface. The surface of this kind will be further referred to as "tearing" morphology and its probable origin will be discussed below.
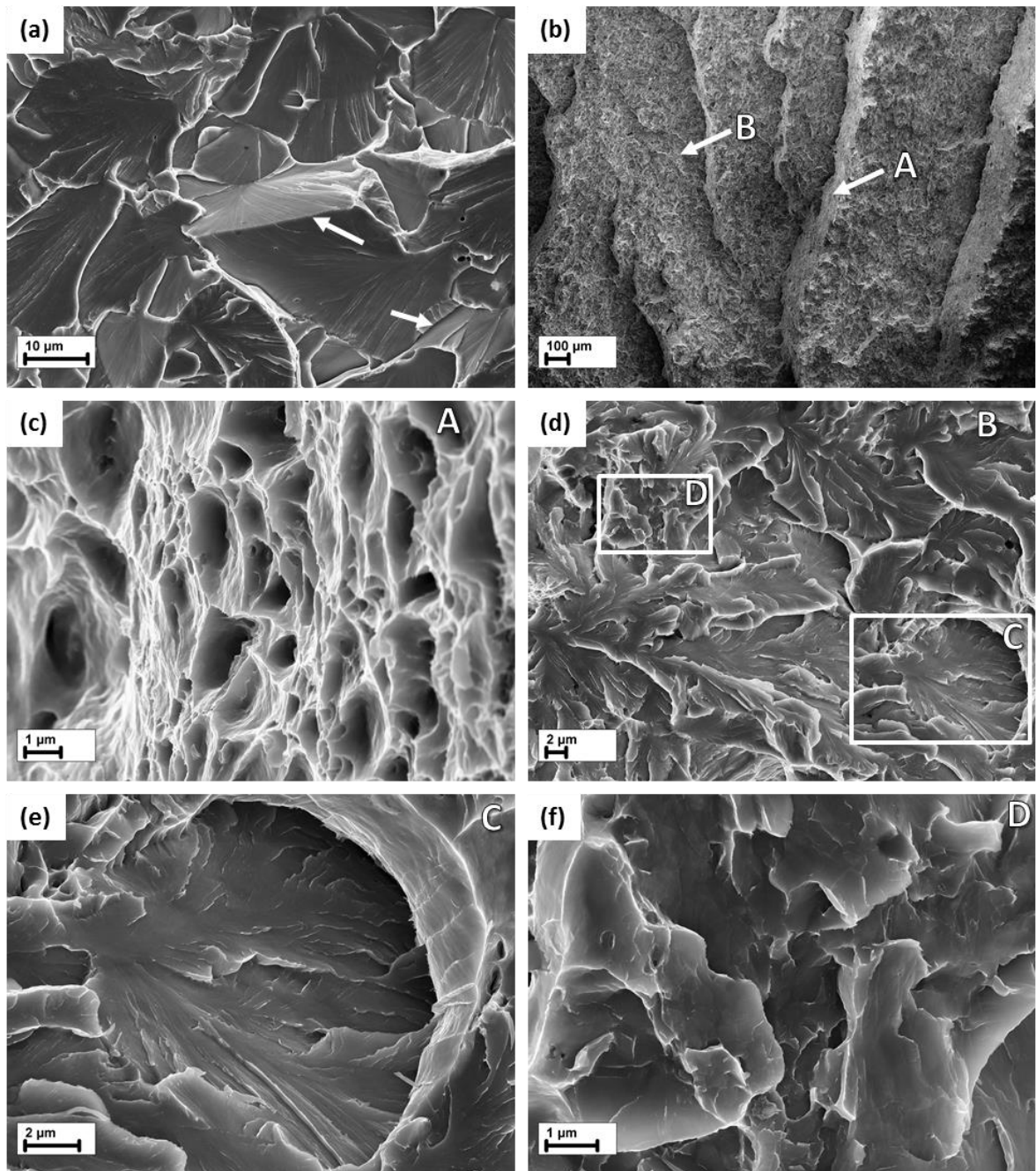

Fig. 5 – Fracture surfaces of the not charged as-received (a) and ECAPed (b-f) specimens after impact testing in liquid nitrogen: (a) – cleavage facets; (b) – terraced relief in the middle part of the fracture surface; (c) – the magnified image of dimpled morphology from the ductile terrace region indicated by arrow "A" in (b); (d) – the magnified image of mixed cleavage/tearing morphology from the brittle terrace region indicated by arrow "B" in (b); (e) and (f) – the magnified images of the cleavage and tearing morphologies from the outlined regions marked as "C" and "D" in (d), respectively.

Hydrogen charging changes the fracture surface appearance dramatically for both the as-received and ECAPed tensile tested specimens. About 50% of the fracture surface area of the hydrogen-charged as-received specimens consists of numerous fisheye defects, Fig. 6a, which are the round-shape regions having the faceted quasi-cleavage morphology and nonmetallic inclusions in their centers, c.f. Fig. 6b and Fig.7. As follows from the primary orientation of river-markings on the facets, the growth of fisheyes occurred in the radial direction from nonmetallic inclusions serving as initiation sites, c.f. arrows in Fig. 6b.
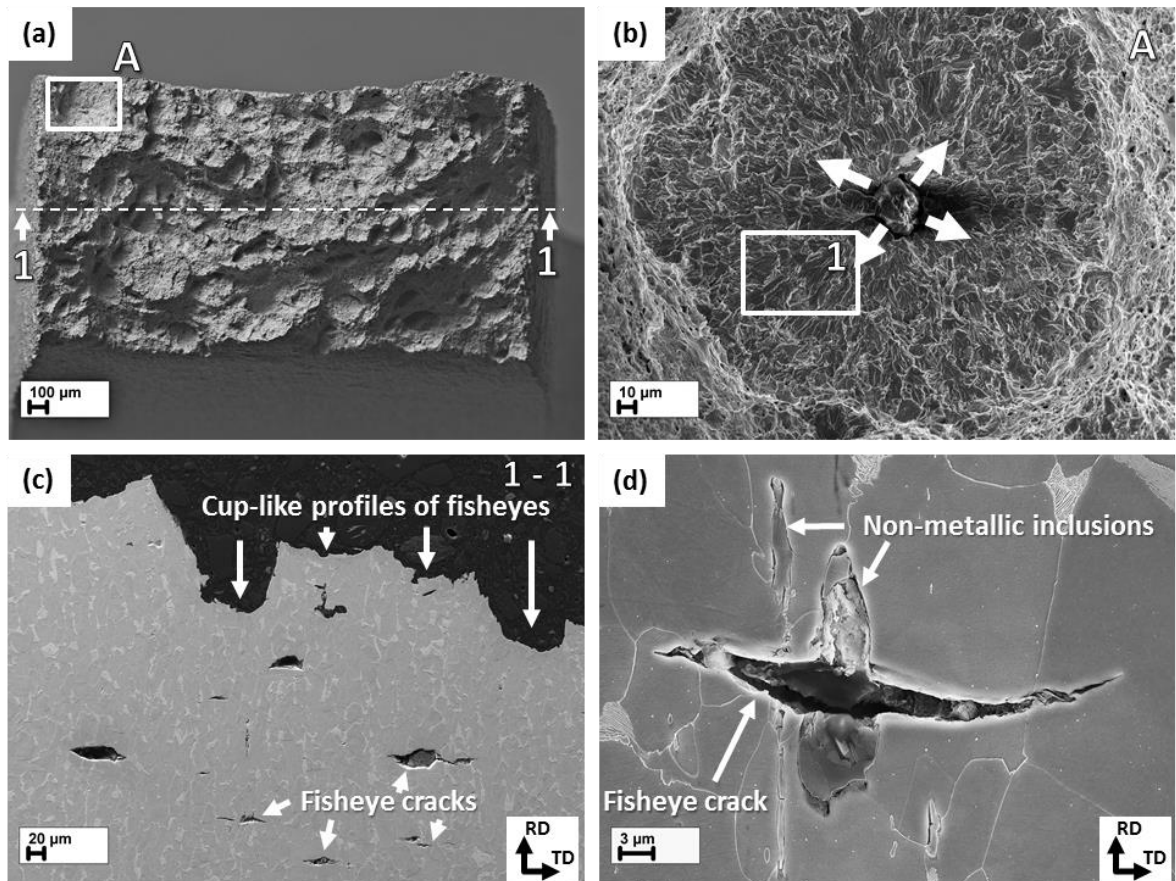

Fig. 6 – Fracture features of the tensile tested hydrogen charged as-received specimen: (a) – full-scale view of the fracture surface; (b) – the magnified image of the fisheye defect from the outlined region marked as "A" in (a); (c) – the cups-like profile of the fracture surface and underlying fisheye cracks on the cross-section taken approximately along the dashed line "1-1" in (a); (d) – the cross-sectional image of the fisheye crack originating at non-metallic inclusion.

The metallographic examination of the fracture surface cross-sections shows that fisheyes have the cup-like profile and are formed by growth and coalescence of the cracks which are readily found beneath the fracture surface, c.f. Fig. 6c. These cracks are approximately parallel to the fracture surface and, in contrast with HICs, are oriented perpendicular to the rolling direction and the tensile axis of the specimens, Fig. 6c, d. It is clear that these cracks originate at

non-metallic inclusions and propagate in a transgranular manner as evidenced by Fig. 6d. Neither such cracks nor the fisheyes were found in the hydrogen-charged as-received specimens, which were degassed before tensile testing. In fact, the fracture surface of the degassed as-received specimens is completely ductile and is the same as that before hydrogen charging, see Fig. 4a, c.

The quasi-cleavage facets on the fisheyes surface have a complex morphology, c. f. Fig. 7. It composed of nearly-flat step-wise terraces with river markings, Fig. 7b-d, presented by straight and Y-shaped tear ridges showed by arrows in Fig. 7b and c, respectively. Besides, there are thin bands or striations approximately perpendicular to the river markings, as indicated by arrows in Fig. 7f. It should be underlined that this morphology is completely different from the cleavage in the as-received and ECAPed specimens tested in liquid nitrogen, Fig. 5a. For example, the facets of fisheyes never have straight boundaries such as those indicated by arrows in Fig. 5a. In common, the differences between cleavage and quasi-cleavage of fisheyes in steel 09G2S are the same as in low-carbon steel S235JR as was described in detail in [37].
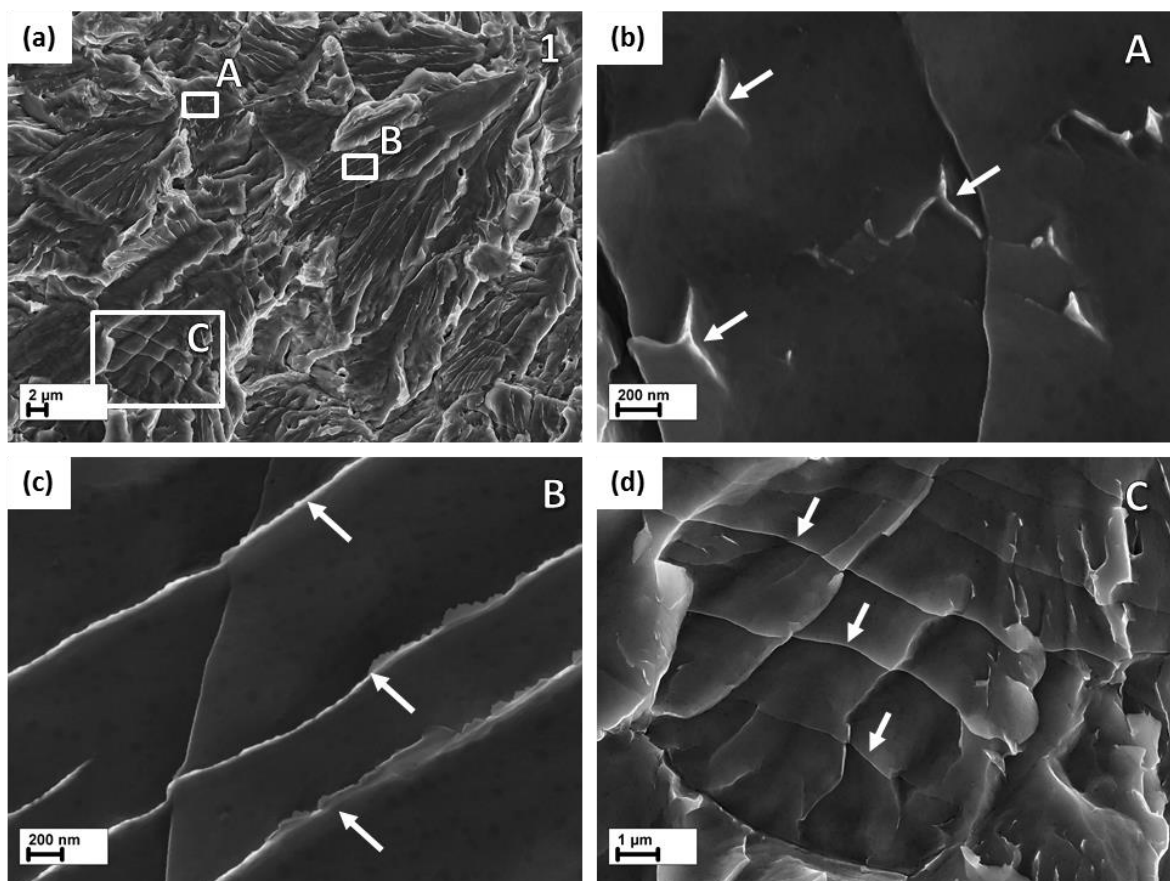

Fig. 7 – Fractographic features of the quasi-cleavage morphology in the hydrogen-charged as-received steel: (a) – the magnified image of the quasi-cleavage facets from the outlined region marked as "1" in Fig. 6b; (b-d) – magnified images representing nearly-flat terraces with Y-shaped (b) and straight (c) tear ridges, and thin bands perpendicular to the river markings (d)

from the outlined regions marked as A, B, and C in (a), respectively. The features of interest are indicated by arrows in each corresponding image.

Similar to the ECAPed specimens tested in liquid nitrogen, the fracture surface of the hydrogen-charged ECAPed specimens is mainly characterized by the brittle terraces having the mixed cleavage/tearing morphology, c. f. Fig. 8a, b, and ductile walls between them, the same as those in Fig. 5b, c. However, in the case of hydrogen embrittled specimens, the amount of cleavage facets is smaller while the portion of torn surfaces is larger in comparison with the low-temperature embrittled ones, Fig. 8b. Besides, the areas with the tearing-only morphology with no cleavage facets are found on the periphery of the fracture surfaces in the hydrogen-charged ECAPed specimens, Fig. 8c, d. Obviously, one of such regions marked as "B" in Fig. 8a and outlined by the dashed line in the Fig. 8c, was the place where fracture initiated as pointed out by the terraces emanating from this region, see arrows in Fig. 8a and c. The diameter of this region is about 1 mm.
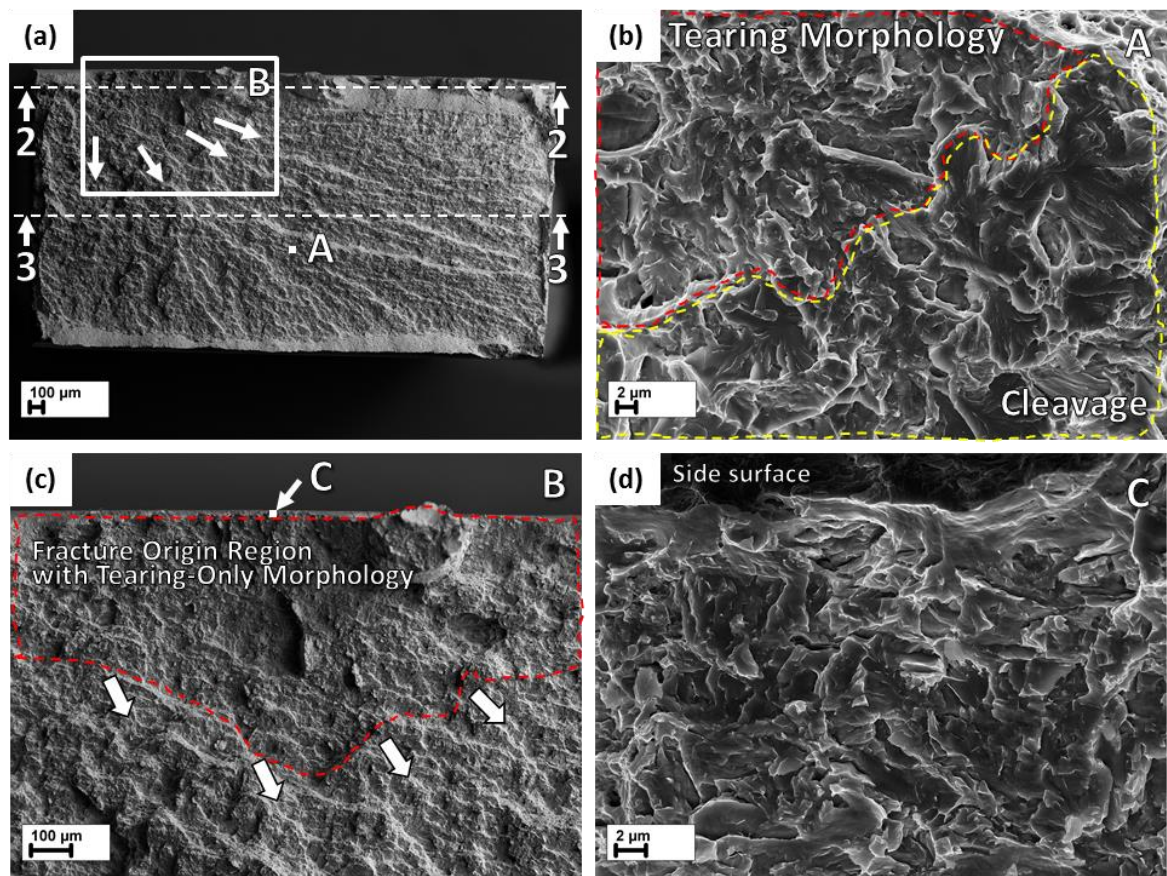

Fig. 8 – The fracture surface of the hydrogen charged ECAPed specimen after tensile testing: (a) – full-scale view; (b) – mixed cleavage/tearing morphology of the brittle terraces from the region marked as "A" in (a); (c) - the magnified image of the fracture origin from the

outlined region marked as "B" in (a); (d) - the magnified image of the tearing-only morphology from the outlined region marked as "C" in (c).

Two cross-sections were prepared from the fracture surface of the hydrogen-charged ECAPed specimen. The first was close to the side surface and the second was cut in the middle part of the specimen as shown schematically by "2-2" and "3-3" dashed lines in Fig. 8a. Both cross-sections demonstrate the fracture surface profile with the mixture of brittle and ductile terraces which are approximately perpendicular to each other and are inclined to the tensile axis of the specimen at about 45°, Fig. 9a, b. Numerous sharp cracks parallel to the brittle terraces can be seen under the fracture surface on the "2-2" cross-section close to the side surface, see arrowheads in Fig. 9a, while on the cross-section "3-3" close to the center they are almost absent, Fig. 9b. This observation indicates that multiple cracking started from the side surface and then one or few of such cracks provoked final fracture occurring by the critical growth of the one major crack in the central part of the specimen. Figure 9a shows that the cracks under the fracture surface are not linked to each other. Thus, it implies that their ductile coalescence occurred at the final fracture stage. The appearance of these cracks shown in Fig. 9c, d is similar to HICs which were found in the hydrogen-charged ECAPed specimens before tensile testing. They are also inclined at ~45° to the specimen surface and are transgranular with respect to the initial ferritic grains of the steel.
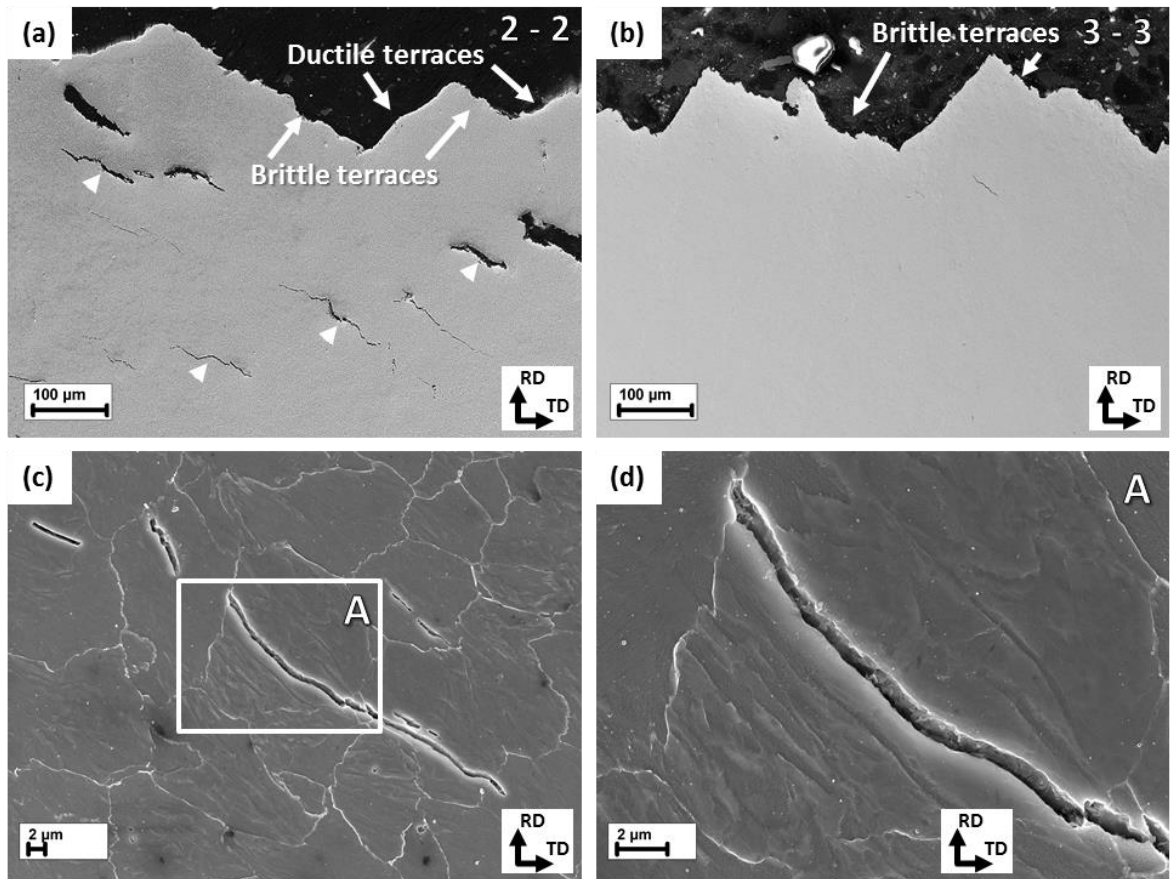
Fig. 9 – Terraced profiles and underlying cracks of the fracture surface of the hydrogen-charged ECAPed specimen: not-etched (a) – near side-surface and (b) – middle part cross-sections of the fracture surface taken approximately along the "2-2" and "3-3" dashed lines in the Fig. 8a, respectively; (c, d) – one of the cracks beneath the fracture surface on the etched "2-2" cross-section at different magnifications.

The specimens subjected to degassing at 200 °C (15 min) prior to testing exhibited the mostly ductile fracture surface. However, several round shaped regions with the "tearing" morphology could be found on the periphery. The diameter of these regions is not higher than 320 μm. One of them is shown at higher magnification in Fig. 10b. This region is located on the terrace which is the part of one of many cracks existing on the side surface of the specimen, see arrows in Fig. 10a. Examination of the side surface showed that these cracks are inclined at ~45° to the tensile axis of the specimen, and their surface is also characterized by the tearing-only morphology. The same cracks are found in the near-side surface cross-section prepared from the fracture surface of the preliminary degassed specimen, c. f. Fig. 10c, d. As can be seen, most of the cracks beneath the fracture surface are wide open and well blunted.
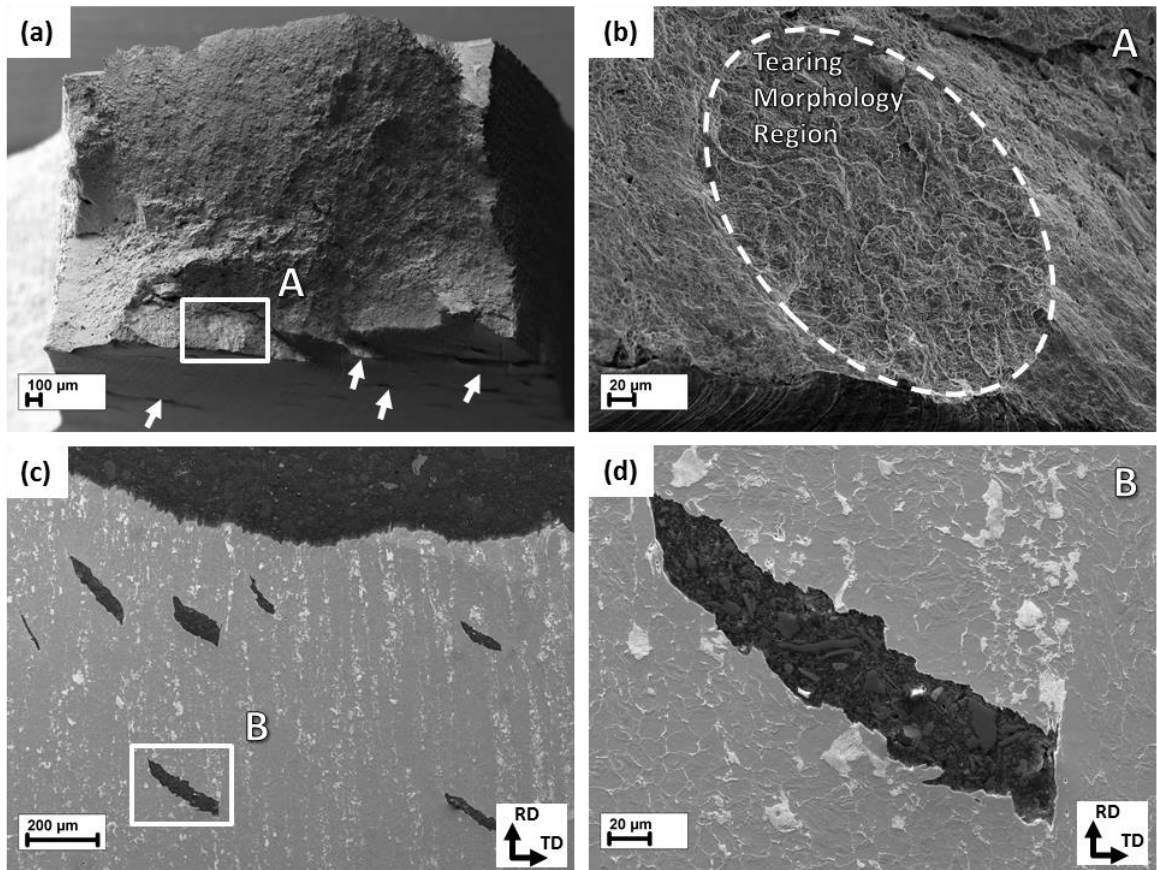
Fig. 10 – Fracture features of the hydrogen-charged ECAPed specimen degassed at 200 °C:
(a) – full-scale view of the fracture surface and side surface cracks indicated by arrows; (b) – the
magnified image of the torn region marked as "A" in (a) and highlighted by an ellipce; (c) –
blunted cracks beneath the fracture surface on the near-side surface cross-section; (d) – the
magnified image of the blunted crack from the region marked as "C" in (e).

Degassing at a higher temperature and longer time prior to mechanical testing results in the
almost complete vanishing of the tearing morphology on the fracture surface, Fig. 11a, b,
although many side surface cracks still demonstrate this kind of relief. The very rare example
(actually the only one) of the torn region with 130 μm diameter is shown in Fig. 11c.
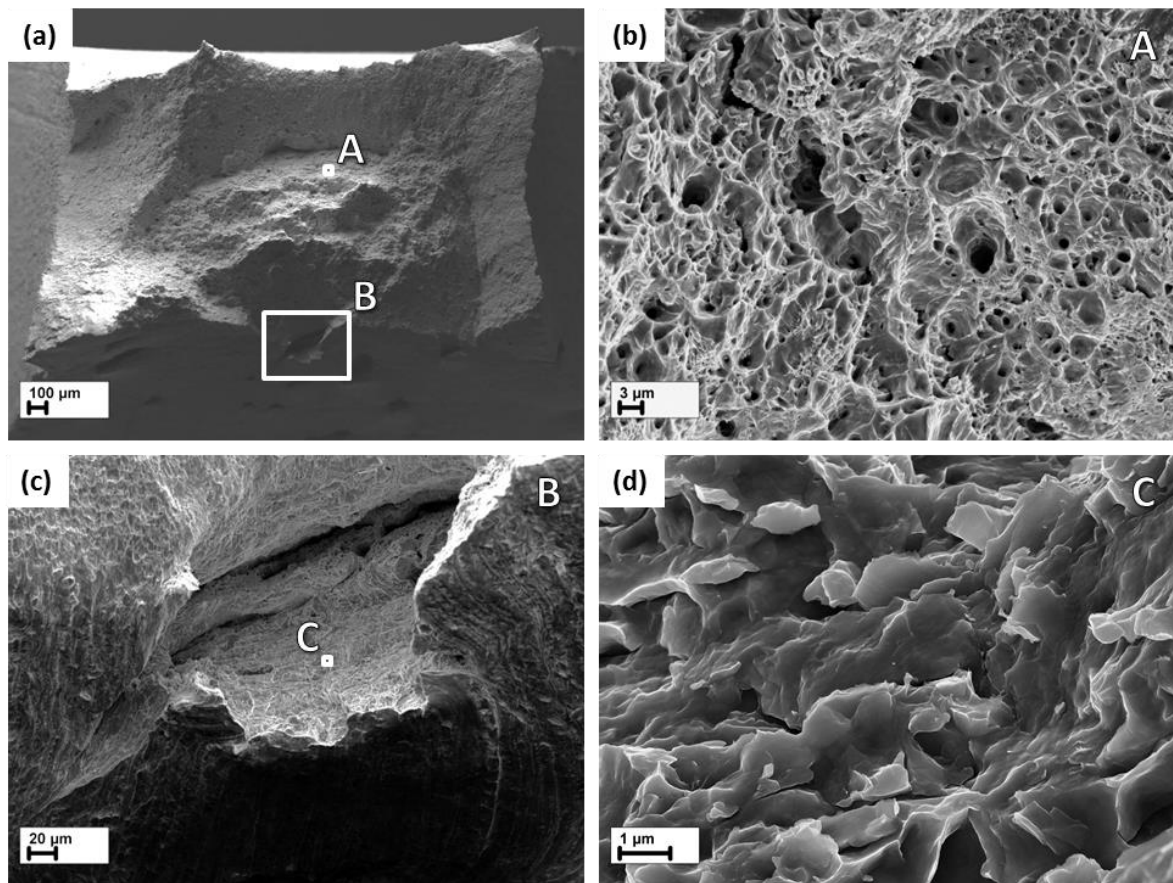
Fig. 11 – Fracture features of the hydrogen-charged ECAPed specimen degassed at 300 °C: (a) – full-scale view of the fracture surface; (b) – the magnified image of the dimpled morphology from the region marked as "A" in (a). (c) – the magnified image of the side surface crack from the region marked as "B" in (a); (d) – the magnified image of the tearing-only morphology from the region marked as "C" in (c);

4. Discussion

The presented results clearly show that after cathodic hydrogen charging both the as-received and ECAPed specimens of the low-carbon steel grade 09G2S exhibit recognizable symptoms of HE, including the appearance of hydrogen-induced defects, the ductility loss and the change of the fracture mode from ductile to brittle. However the details of these HE features as well as AE behavior are distinctly different for the two types of specimens of the nominally the same steel.

The experiments with degassed specimens revealed that mechanical properties and fracture surface of the hydrogen-charged steel in both as-received and ECAPed state could be completely recovered by removing diffusible hydrogen from the specimens. It was noticed that the longer duration and higher temperature of degassing were required for successful removing diffusible hydrogen from the ECAPed steel. Thus, it is concluded that HICs, which are produced at present hydrogen charging conditions, do not affect the tensile mechanical properties and fracture

surface of both the as-received and ECAPed 09G2S steels if the concentration of diffusible hydrogen in these steels is low enough. Consequently, diffusible hydrogen plays the key role in HE of the investigated steels.

4.1. Acoustic emission behavior and the mechanism of hydrogen-assisted cracking in the as-received steel

According to fractographic observations, the formation of fisheyes occurs just during the tensile test. Furthermore, it necessarily requires the presence of diffusible hydrogen in the as-received steel. This statement is corroborated by the experimental fact that the fisheyes are not produced if diffusible hydrogen is removed from the steel before tensile testing. As was shown by the metallographic examination, the fisheyes are formed due to the growth of transgranular cracks originating at non-metallic inclusions, Fig. 6d, which are commonly found in the centers of fisheyes, Fig. 6b. Such cracks, as well as fisheyes, are oriented normally to the rolling direction of the steel and to the HICs nucleating during hydrogen charging before the tensile test. This means that fisheyes are not the result of the extension of HICs. Instead, fisheyes are produced by propagation of newly formed cracks originating in the course of tensile deformation, though the HICs apparently can sometimes serve as nuclei for the fisheyes. Propagation of the fisheye cracks during tensile testing is accompanied by the formation of the fracture surface having the specific faceted quasi-cleavage morphology, c.f. Fig. 7. However, this process does not produce any significant AE. This is witnessed by the fact that the total AE energy accumulated during tensile tests of the as-received specimens does not depend on whether or not the fisheyes were formed in the steel, c.f. Table 2.

The weak AE response from HAC in the as-received specimens means that the fisheye crack growth and the associated formation of quasi-cleavage fracture surface are not accompanied by the significant rapid energy release as it would be reasonably expected and regularly reported for brittle fracture. This suggests that the mechanism of fisheye cracking differs from the common brittle fracture behavior. Indeed, it was shown that quasi-cleavage morphology on the fisheye surface is completely different from cleavage, Fig. 5a, which occurs in this steel due to cold embrittlement. This observation is consistent with the results of others investigations [3,8,9,38–41] indicating that quasi-cleavage or cleavage-like fracture surfaces in hydrogen embrittled mild steels and iron are distinctly different in both the morphology and the formation mechanism from the cleavage or from what is commonly termed quasi-cleavage. The latter is usually observed in high-strength martensitic steels. It is cleavage by nature because its facets have {001} orientation as was shown by Beachem [42]. Many authors have shown that crystallographic orientation of quasi-cleavage facets in hydrogen-embrittled pure iron and steel corresponds to {110} and less often to {112} planes [38–41] instead of {001} planes in

cleavage. It was also found that quasi-cleavage facets on the fisheye surface have a two times lower misorientation angle and a more curved profile in comparison with these for cleaved ones [37]. Common features of such facets are the striation-like bands perpendicular to the crack growth direction [3,38,40,41] and straight [8] or Y-shaped tear ridges [3], which are not found on the "original" quasi-cleavage or true cleavage fracture surfaces. Very similar morphological elements have been found in the present study on the surface of fisheyes, e.g., Fig. 7. The exact mechanism of fisheye crack growth and formation of their quasi-cleavage morphology has yet to be understood. However, plenty of evidence [2–4,8,9] indicates that plastic deformation affected by hydrogen is pivotal in this process. Particularly, the need of plastic deformation for initiation of fisheye formation has frequently been reported [1,30,43]. If HAC occurs due to a kind of localized MVC process and the cleavage-like morphology is formed by either of scenarios proposed by Lynch [3], Martin et al. [8] or Neeraj et al. [9] (see Introduction), the fisheye crack growth should be relatively slow if compared with cleavage cracking. Indeed, the significant energy release during the short period of time is unlikely from the process of such kind. This can be a plausible reason for the apparent absence of AE related to HE in the as-received specimens.

Finally, it should be noticed that although there is no doubt that the fisheye cracking process generates AE, due to the plastic origin on this strongly localized process, the associated AE is significantly smaller than AE emanating from uniform plastic deformation or possibly even smaller compared to the background noise. The use of advanced AE signal processing techniques such as wavelet-based phase picking [44], spectral noise gating [45], cluster analysis [46] and others helping to improve the signal-to-noise ratio and distinguish between the sources of different kinds can probably resolve the specific signals from forming fisheyes. This will be done in the further dedicated study and reported elsewhere.

4.2. Acoustic emission behavior and the mechanism of hydrogen-assisted cracking in the ECAPed steel

The fracture process of the hydrogen-charged ECAPed specimens is admittedly more complex. The fracture mechanism after ECAP differs from that in the as-received steel. The detailed analysis of results is provided below to shed light on this mechanism and to identify the main sources of AE.

Three kinds of morphologies have been observed on the fracture surface of the hydrogen-charged ECAPed steel: 1) the ductile dimpled relief, Fig. 5c, 2) the cleavage facets, Fig. 5e, and 3) the smooth curved surfaces with tear ridges referred here to as "tearing" morphology, Fig. 5f.

The analysis of the cross-sections of the hydrogen embrittled ECAPed specimens allowed to conclude that the formation of ductile walls between brittle terraces is the very final event at

the fracture process because the brittle cracks beneath the fracture surface are mainly not linked with each other, Fig. 9a. Thus, the influence of ductile rapture on the AE signal recorded before the final break of the specimen should be negligible.

The regions of the tearing-only morphology have been found in the degassed specimens, Fig. 10 and 11. It was established that these regions are produced by the growth of the side surface cracks. Since the cleavage was not found in the degassed specimens, obviously *the propagation of the cracks resulting in the formation of tearing regions is the main source of the burst AE during the deformation of the degassed ECAPed specimens until the final fracture*, Fig. 3f. This conclusion is confirmed by the lower value of the total AE energy accumulated before fracture in the ECAPed specimen which was degassed at 300 °C, Table 2. The much lower amount of tearing morphology has been found in this specimen in comparison with the one degassed at 200 °C.

As follows from the AE behavior in Fig. 3d and f the intensive cracking starts at very low stress almost immediately after onset of loading of the specimens. Hence the fracture of the hydrogen embrittled ECAPed specimens begins at the stress well below yield point and occurs by the sub-critical growth of the multiple side surface cracks producing the regions with tearing-only morphology on the periphery part of the fracture surface. When the size of such cracks becomes essentially big, the local criteria of brittle fracture are met, and unstable critical crack growth occurs. It is in some measure evidenced by the metallographic examination which showed that no secondary cracks beneath the fracture surface are found in the bulk part of the specimen. Another good illustration of proposed scenario is provided in Fig. 8c where it can be seen that many brittle terraces having mixed tearing/cleavage relief originate at the boundary of the near-side surface region with the dominated tearing morphology. Thus the critical crack growth in the hydrogen-charged ECAPed specimens is accompanied by the formation of the fracture surface featuring the mixed cleavage/tearing morphology. According to many previous studies the cleavage fracture is recognized as a strong source of AE. In a good agreement with that, the total energy of AE in the hydrogen-charged specimens is about 2-3 orders of magnitude higher in comparison with the degassed ones which fracture surface does not contain cleavage facets. Therefore, in the case of hydrogen charged ECAPed specimens the total AE energy accumulated during the whole test, ΣE_{AE}, includes the energy of AE from: (i) the sub-critical crack growth characterized by the tearing fracture mode and by the gradual increase of AE energy at the onset of loading, c.f. Fig. 3d; (ii) the critical crack growth exhibiting the mixed tearing/cleavage fracture morphology and accompanying by the dramatic increase in the AE energy just before fracture; (iii) final ductile rupture of the walls of metal between the brittle terraces at the break.

Figure 3f illustrates that the degassed specimens show no substantial increase of the AE intensity just before fracture; the AE disappears almost completely before necking sets in. On the other hand, no cleavage fracture has been observed in these specimens. Thus, the brittle critical crack growth does not occur in the degassed specimens, and only sub-critical cracking and ductile rupture contribute to the ΣE_{AE} value. It was shown that at a higher degassing temperature and, consequently, at lower diffusible hydrogen concentration in the steel, the torn regions have a smaller size. This suggests that the rate of the sub-critical crack growth depends on the concentration of diffusible hydrogen in the ECAPed steel. Considering a relatively short time of tensile testing, the side cracks do not have enough time to grow up to the critical size in the degassed specimens having the quite low concentration of diffusible hydrogen. Hence, they blunt by plastic deformation as illustrated in Fig. 10c, d. Indeed, Figures 10b and 8c show that the diameter of the largest torn region on the fracture surface of the specimen degassed at 200 °C is about three times smaller than the critical one in the not degassed specimen, Figs. 8c. As follows from AE data in Fig. 3f, the growth of the cracks producing tearing morphology stops at the necking point and only blunting occurs during further straining in the neck.

It is found that all side surface cracks are: (i) inclined at ~45° to the extrusion direction and to the tensile axis of the specimen, i.e., aligned with the shear plane of the last pressing operation; (ii) aligned with the direction of grain elongation caused by simple shear during ECAP; (iii) transgranular with respect to the initial ferritic grains. These observations suggest that they are identical to HICs which are formed during hydrogen charging in the ECAPed steel. The existence of the specific shear plane predefined by the simple shear geometry of the die with two intersecting at 90° channels facilitates the formation of HICs along this plane of the last pressing operation. Thus, it can be concluded that HAC of the hydrogen-charged ECAPed specimens occurs by the extension of the HICs pre-existed in the microstructure before tensile testing. Alternatively, nucleation and growth of new cracks of the same kind are also possible. The growth of such cracks produces the distinct fracture morphology featured by the smooth curved surfaces with tear ridges. Despite the transgranular path of the cracks, this morphology is markedly different from cleavage. A small fraction of this kind of fracture surface is also present in the low-temperature embrittled ECAPed specimens which were not hydrogen charged. It means that hydrogen promotes conventional brittle fracture while it does not produce any unique fracture surface features in the ECAPed steel as it does, for example, in the as-received one. However, in the presence of hydrogen, the tearing morphology prevails even during the critical crack growth. Revealing the exact formation mechanism of such a fracture surface requires additional thorough examination of the microstructure along the crack path, employing EBSD and other high-resolution methods. This is the beyond the scope of the present paper and will be

a subject of future research. However, it can be plausibly supposed that these cracks grow along the dislocation sub-structure (cell) boundaries which are abundantly present in the microstructure of the ECAPed steel as was shown in Fig. 2b. The cells (or sub-grains), as well as cracks, are stretched along the shear direction of the ECAP. It has been well understood that dislocations and low-angle dislocation boundaries are strong traps of hydrogen. A particularly high local hydrogen concentration can be achieved at these traps giving rise to the high average hydrogen concentration in a whole specimen as well, c.f. Table 2. Hence, trapped hydrogen can weaken the dislocation sub-boundaries, making them susceptible to easy crack nucleation and growth.

The strong transient AE during HAC in the ECAPed steel witnesses for the rapid release of elastic energy accompanying the formation of the tearing morphology on the fracture surface. As it has been discussed in Introduction, such a morphological feature is inherent to "brittle" mechanisms of HAC like HEDE. Another argument in favor of the "brittle" mode of HAC is based on the observation that hydrogen does not produce new features on the fracture surface of the ECAPed steel in comparison with the ordinary brittle fracture of the ECAPed steel. According to the HEDE theory, hydrogen can reduce the strength of the bonds between metal atoms. Thereby the brittle fracture along the dislocation boundaries is reasonably expected as they likely contain the high concentration of diffusible hydrogen.

5.   Summary and conclusions.

The experimental findings of the present study indicate that, depending on the fracture mode, HAC does not always produce a high-energy AE as the typical brittle fracture does. This fact can be related to the complex nature of HAC. This should be accounted when the AE method is used for non-destructive testing and monitoring of industrial components susceptible to the influence of hydrogen. On the other hand, the AE method is found to be a promising tool for the further investigation of fracture and deformation processes associated with HE. Another important point of the present research is that the HAC mechanism can be changed by modification of the steel microstructure, for example, by severe plastic deformation. However, the exact reasons for these observations have yet to be understood.

The main conclusions of the present study can be summarized as follows:

1.   The extent of influence of HICs on mechanical properties and fracture surface appearance of the steel grade 09G2S in both as-received and ECAPed states depends strongly on the concentration of diffusible hydrogen. The harmful effect of HICs can be completely eliminated by a proper degassing procedure.

2.   The AE behavior tensile testing of hydrogen embrittled steel is strongly influenced by the fracture mode of HAC. In particular, the quasi-cleavage fisheye cracking in the hydrogen-

charged low-strength low-alloy steel produces substantially weaker AE in comparison with HAC which accompanied by the formation of torn and cleavage fracture surface in the same steel preliminary subjected to ECAP. Thus the AE method can be used for recognizing the fracture modes of HAC and distinguishing between them.

3. The HAC of the ECAPed steel grade 09G2S starts at the quasi-elastic stage of tensile testing and occurs by the brittle sub-critical growth of the side surface cracks producing the specific tearing fracture surface morphology and strong AE. This process is followed by the critical crack growth accompanied by mixed tearing/cleavage fracture and the dramatic increase in the AE energy. It is suggested that this kind of HAC is the result of hydrogen-enhanced decohesion along the low-angle dislocation boundaries created during ECAP.

4. HAC of the as-received 09G2S steel occurs transgranularly resulting in the formation of fracture surface consisting of fisheye defects with the faceted quasi-cleavage morphology which is completely different from the cleavage patterns found in the same steel tested in liquid nitrogen. Because of the low AE response, it is suggested that HELP, AIDE or NVC mechanisms can be responsible for the HAC in the as-received low-strength 09G2S steel.

References

[1]   M.R. Louthan, Hydrogen Embrittlement of Metals: A Primer for the Failure Analyst, J. Fail. Anal. Prev. 8 (2008) 289–307. doi:10.1007/s11668-008-9133-x.

[2]   I.M. Robertson, P. Sofronis, A. Nagao, M.L. Martin, S. Wang, D.W. Gross, et al., Hydrogen Embrittlement Understood, Metall. Mater. Trans. A. 46 (2015) 2323–2341. doi:10.1007/s11661-015-2836-1.

[3]   S.P. Lynch, Hydrogen embrittlement phenomena and mechanisms, Corros. Rev. 30 (2012) 63–133. doi:10.1515/corrrev-2012-0502.

[4]   M. Nagumo, Fundamentals of Hydrogen Embrittlement, Springer Singapore, Singapore, 2016. doi:10.1007/978-981-10-0161-1.

[5]   W. Gerberich, Modeling hydrogen induced damage mechanisms in metals, in: R.P.

Gangloff, B.P. Somerday (Eds.), Gaseous Hydrog. Embrittlement Mater. Energy Technol. Vol. 2 Mech. Model. Futur. Dev., Woodhead Publishing Limited, Philadelphia, 2012: pp. 209–246. doi:10.1016/B978-0-85709-536-7.50008-8.

[6]   S.L. Lee, D.J. Unger, A decohesion model of hydrogen assisted cracking, Eng. Fract. Mech. 31 (1988) 647–660. doi:10.1016/0013-7944(88)90107-5.

[7]   J. Song, W. a Curtin, Atomic mechanism and prediction of hydrogen embrittlement in iron., Nat. Mater. 12 (2012) 145–51. doi:10.1038/nmat3479.

[8]   M.L. Martin, J.A. Fenske, G.S. Liu, P. Sofronis, I.M. Robertson, On the formation and nature of quasi-cleavage fracture surfaces in hydrogen embrittled steels, Acta Mater. 59 (2011) 1601–1606. doi:10.1016/j.actamat.2010.11.024.

[9]   T. Neeraj, R. Srinivasan, J. Li, Hydrogen embrittlement of ferritic steels: Observations on deformation microstructure, nanoscale dimples and failure by nanovoiding, Acta Mater. 60 (2012) 5160–5171. doi:http://dx.doi.org/10.1016/j.actamat.2012.06.014.

[10]   Y. Ogawa, D. Birenis, H. Matsunaga, A. Thøgersen, Ø. Prytz, O. Takakuwa, et al., Multi-scale observation of hydrogen-induced, localized plastic deformation in fatigue-crack propagation in a pure iron, Scr. Mater. 140 (2017) 13–17. doi:10.1016/j.scriptamat.2017.06.037.

[11]   M.L. Martin, I.M. Robertson, P. Sofronis, Interpreting hydrogen-induced fracture surfaces in terms of deformation processes: A new approach, Scr. Mater. 59 (2011) 3680–3687. doi:10.1016/j.actamat.2011.03.002.

[12]   P.J. Ferreira, I.M. Robertson, H.K. Birnbaum, Hydrogen effects on the interaction between dislocations, Acta Mater. 46 (1998) 1749–1757. doi:10.1016/S1359-6454(97)00349-2.

[13]   B.S. Kumar, V. Kain, M. Singh, B. Vishwanadh, Influence of hydrogen on mechanical properties and fracture of tempered 13 wt% Cr martensitic stainless steel, Mater. Sci. Eng. A. 700 (2017) 140–151. doi:10.1016/j.msea.2017.05.086.

[14]   P. Novak, R. Yuan, B.P. Somerday, P. Sofronis, R.O. Ritchie, A statistical, physical-based, micro-mechanical model of hydrogen-induced intergranular fracture in steel, J. Mech. Phys. Solids. 58 (2010) 206–226. doi:10.1016/j.jmps.2009.10.005.

[15]   M.B. Djukic, V. Sijacki Zeravcic, G.M. Bakic, A. Sedmak, B. Rajicic, Hydrogen damage of steels: A case study and hydrogen embrittlement model, Eng. Fail. Anal. 58 (2015) 485–498. doi:10.1016/j.engfailanal.2015.05.017.

[16]   M. Koyama, C.C. Tasan, E. Akiyama, K. Tsuzaki, D. Raabe, Hydrogen-assisted decohesion and localized plasticity in dual-phase steel, Acta Mater. 70 (2014) 174–187. doi:10.1016/j.actamat.2014.01.048.

[17] A. Vinogradov, D. Orlov, A. Danyuk, Y. Estrin, Effect of grain size on the mechanisms of plastic deformation in wrought Mg-Zn-Zr alloy revealed by acoustic emission measurements, Acta Mater. 61 (2013) 2044–2056. doi:10.1016/j.actamat.2012.12.024.

[18] A. Vinogradov, D. Orlov, A. Danyuk, Y. Estrin, Deformation mechanisms underlying tension-compression asymmetry in magnesium alloy ZK60 revealed by acoustic emission monitoring, Mater. Sci. Eng. A. 621 (2015) 243–251. doi:10.1016/j.msea.2014.10.081.

[19] X. Chen, W.W. Gerberich, Evidence for 1μm size instabilities in hydrogen-assisted cracking of Fe3%Si crystals, Scr. Metall. 22 (1988) 1499–1502. doi:10.1016/S0036-9748(88)80027-9.

[20] X. Chen, W.W. Gerberich, The Kinetics and Micromechanics of Hydrogen- Assisted Cracking in Fe-3 Pct Si Single Crystals, Metall. Trans. A. 22 (1991) 59–70. doi:10.1007/BF03350949.

[21] H.L. Dunegan, A.S. Tetelman, Non-Destructive characterization of hydrogen-embrittlement cracking by acoustic emission techniques, Eng. Fract. Mech. 2 (1971) 387–402. doi:10.1016/0013-7944(71)90021-x.

[22] D.D. Dedhia, W.E. Wood, Application of acoustic emission analysis to hydrogen-assisted cracking, Mater. Sci. Eng. 49 (1981) 263–273. doi:10.1016/0025-5416(81)90121-x.

[23] A.W. Vasudevan, R. Stout, R. D. Pense, Hydrogen-Assisted Cracking in HSLA Pipeline Steels, Weld. J. 60 (1981) 155–168.

[24] R. Padmanabhan, N. Suriyayothin, W. Wood, Grain size-acoustic emission relationships in hydrogen induced delayed cracking, Metall. Mater. Trans. A. 14 (1983) 2357–2362. doi:10.1007/bf02663311.

[25] R. Jones, M. Friesel, W. Gerberich, Acoustic emission from integranular subcritical crack growth, Metall. Mater. Trans. A. 20 (1989) 637–648. doi:10.1007/bf02667582.

[26] S. Carpenter, D. Smith, The effects of cathodic charging on the acoustic emission generated by intergranular cracking in sensitized 304 stainless steel, Metall. Mater. Trans. A. 21 (1990) 1933–1939. doi:10.1007/bf02647241.

[27] A.K. Bhattacharya, N. Parida, P.C. Gope, Monitoring hydrogen embrittlement cracking using acoustic emission technique, J. Mater. Sci. 27 (1992) 1421–1427. doi:10.1007/bf00542897.

[28] E.D. Merson, M.M. Krishtal, D.L. Merson, A.A. Eremichev, A. Vinogradov, Effect of strain rate on acoustic emission during hydrogen assisted cracking in high carbon steel, Mater. Sci. Eng. A. 550 (2012) 408–417. doi:http://dx.doi.org/10.1016/j.msea.2012.04.094.

[29] Y. You, Q. Teng, Z. Zhang, Q. Zhong, The effect of hydrogen on the deformation

mechanisms of 2.25Cr-1Mo low alloy steel revealed by acoustic emission, Mater. Sci. Eng. A. 655 (2016) 277–282. doi:10.1016/j.msea.2016.01.006.

[30] E. Merson, A. Vinogradov, D.L. Merson, Application of acoustic emission method for investigation of hydrogen embrittlement mechanism in the low-carbon steel, J. Alloys Compd. 645 (2015) S460–S463. doi:10.1016/j.jallcom.2014.12.083.

[31] W.W. Gerberich, R.H. Jones, M.A. Friesel, A. Nozue, Acoustic emission monitoring of stress corrosion cracking, Mater. Sci. Eng. A. 103 (1988) 185–191. doi:10.1016/0025-5416(88)90565-4.

[32] E. Merson, D. Merson, A. Vinogradov, Acoustic emission monitoring of fracture process stages in Hydrogen embrittled Highcarbon Steel, in: 12th Int. Conf. Slov. Soc. Non-Destructive Test. Appl. Contemp. Non-Destructive Test. Eng. ICNDT 2013 - Conf. Proc., 2013: pp. 657–664.

[33] A.E. Andreikiv, N. V Lysak, V.R. Skal'skii, I.L. Parasyuk, O.N. Sergienko, Acoustic-emission monitoring of hydrogen cracking in metals and alloys, Mater. Sci. 28 (1993) 378–382. doi:10.1007/bf00723217.

[34] R.Z. Valiev, T.G. Langdon, Principles of equal-channel angular pressing as a processing tool for grain refinement, Prog. Mater. Sci. 51 (2006) 881–981. doi:10.1016/j.pmatsci.2006.02.003.

[35] C.R. Heiple, S.H. Carpenter, Acoustic emission produced by deformation of metals and alloys - A review., J. Acoust. Emiss. 6 (1987) 177–204.

[36] A. Vinogradov, Acoustic emission in ultra-fine grained copper, Scr. Mater. 39 (1998) 797–805. doi:10.1016/S1359-6462(98)00180-8.

[37] E. Merson, A.V. Kudrya, V.A. Trachenko, D. Merson, V. Danilov, A. Vinogradov, Quantitative characterization of cleavage and hydrogen-assisted quasi-cleavage fracture surfaces with the use of confocal laser scanning microscopy, Mater. Sci. Eng. A. 665 (2016) 35–46. doi:10.1016/j.msea.2016.04.023.

[38] N. Takano, K. Kidani, Y. Hattori, F. Terasaki, Fracture surface of hydrogen embrittlement in iron single crystals, Scr. Metall. Mater. 29 (1993) 75–80. doi:10.1016/0956-716X(93)90257-S.

[39] Y. Kikuta, T. Araki, T. Kuroda, Analysis of Fracture Morphology of Hydrogen-Assisted Cracking in Steel and Its Welds, in: B.M. Strauss, W.H. Cullen (Eds.), Fractography Fail. Anal., 1978: pp. 107–127. doi:10.1520/STP38088S.

[40] F. Nakasato, I. Bernstein, Crystallographic and fractographic studies of hydrogen- induced cracking in purified iron and iron- silicon alloys, Metall. Mater. Trans. A. 9 (1978) 1317–1326. doi:10.1007/bf02652256.

[41] A. Kimura, H. Kimura, Hydrogen embrittlement in high purity iron single crystals, Mater. Sci. Eng. 77 (1986) 75–83. doi:10.1016/0025-5416(86)90355-1.

[42] C.D. Beachem, Orientation of cleavage facets in tempered martensite (quasi-cleavage) by single surface trace analysis, Metall. Trans. 4 (1973) 1999–2000. doi:10.1007/BF02665434.

[43] G. Vibrans, Fisheyes in rolled steel exposed to hydrogen at room temperature, Metall. Trans. A. 8 (1977) 1318–1320. doi:10.1007/BF02643849.

[44] E. Pomponi, A. Vinogradov, A. Danyuk, Wavelet based approach to signal activity detection and phase picking: Application to acoustic emission, Signal Processing. 115 (2015) 110–119. doi:10.1016/j.sigpro.2015.03.016.

[45] A. Vinogradov, A. V. Danyuk, D.L. Merson, I.S. Yasnikov, Probing elementary dislocation mechanisms of local plastic deformation by the advanced acoustic emission technique, Scr. Mater. 151 (2018) 53–56. doi:10.1016/j.scriptamat.2018.03.036.

[46] E. Pomponi, A. Vinogradov, A real-time approach to acoustic emission clustering, Mech. Syst. Signal Process. 40 (2013) 791–804. doi:10.1016/j.ymssp.2013.03.017.